Published for SISSA by Springer

Received: January 29, 2020
Revised: May 30, 2020
Accepted: June 24, 2020
Published: July 24, 2020

Heating neutron stars with GeV dark matter

Wai-Yee Keung,[a] **Danny Marfatia**[b] **and Po-Yan Tseng**[c]

[a] *Department of Physics, University of Illinois at Chicago, Illinois 60607 U.S.A.*
[b] *Department of Physics and Astronomy, University of Hawaii, Honolulu, HI 96822, U.S.A.*
[c] *Department of Physics and IPAP, Yonsei University, Seoul 03722, Republic of Korea*

E-mail: keung@uic.edu, dmarf8@hawaii.edu, tpoyan1209@gmail.com

Abstract: An old neutron star (NS) may capture halo dark matter (DM) and get heated up by the deposited kinetic energy, thus behaving like a thermal DM detector with sensitivity to a wide range of DM masses and a variety of DM-quark interactions. Near future infrared telescopes will measure NS temperatures down to a few thousand Kelvin and probe NS heating by DM capture. We focus on GeV-mass Dirac fermion DM (which is beyond the reach of current DM direct detection experiments) in scenarios in which the DM capture rate can saturate the geometric limit. For concreteness, we study (1) a model that invokes dark decays of the neutron to explain the neutron lifetime anomaly, and (2) a framework of DM coupled to quarks through a vector current portal. In the neutron dark decay model a NS can have a substantial DM population, so that the DM capture rate can reach the geometric limit through DM self-interactions even if the DM-neutron scattering cross section is tiny. We find NS heating to have greater sensitivity than multi-pion signatures in large underground detectors for the neutron dark decay model, and sub-GeV gamma-ray signatures for the quark vector portal model.

Keywords: Beyond Standard Model, Chiral Lagrangians

ArXiv ePrint: 2001.09140

https://doi.org/10.1007/JHEP07(2020)181

JHEP07(2020)181

Contents

1 Introduction **1**

2 Dark matter capture in neutron stars **2**

3 Temperature evolution **5**

4 Neutron dark decay model **8**
- 4.1 Model and NS equation of state 8
- 4.2 DM-DM scattering cross section 11
- 4.3 DM-neutron elastic scattering and annihilation cross sections 14
- 4.4 Results 14
  - 4.4.1 χ is DM 15
  - 4.4.2 $\bar{\chi}$ is DM 16

5 Quark vector current portal dark matter **17**
- 5.1 DM-nucleon scattering cross section 17
- 5.2 Chiral Lagrangian and DM annihilation 18
- 5.3 Results 19

6 Summary **21**

JHEP07(2020)181

1 Introduction

Dark matter (DM) may have a variety of interactions with SM particles and with DM itself, but with strengths that have evaded observation. A neutron star (NS) orbits through large fluxes of halo DM particles which may lose their energy via their interactions with the NS and become gravitationally bound to it. The high density and strong gravity of a NS may be able to compensate the feeble DM interactions and enhance the DM capture rate. The capture of halo DM by a NS had been extensively studied [1–7]. During the capture process, the strong gravitational potential of the NS accelerates the DM to more than half the speed of light, and DM-neutron scattering releases this kinetic energy to heat up the NS. Consequently, the NS temperature evolution will deviate from the standard cooling profile. A possible observable signal of DM capture by a NS is the detection of unexpectedly hot old neutron stars. The temperature of an old neutron star can be heated by ~ 100 K to ~ 2000 K, which is within the near-infrared band of the blackbody spectrum. The thermal emissions from nearby (within 100 pc), faint and isolated NS can be probed by upcoming infrared telescopes such as the James Webb Space Telescope (JWST), the Thirty Meter Telescope, and the European Extremely Large Telescope [3].

A DM-neutron cross section of $\sim 2 \times 10^{-45}$ cm^2 is large enough to heat up an old neutron star to ~ 1000 K for DM masses between GeV and PeV. For DM lighter than a GeV, the capture rate is suppressed by Pauli blocking, while for DM heavier than a PeV, multiple scattering is necessary to slow down the halo DM particles. However, the total capture rate must lie below the geometric limit, which corresponds to all the ambient halo DM within the geometric area of the NS being captured.

We study scenarios with three aspects: (1) the DM is of GeV mass, which makes direct detection problematic, (2) the DM is a Dirac fermion, so that it matters whether the particle or the antiparticle is the DM, and (3) the DM capture rate can reach the geometric limit. Specifically, we examine NS heating in the neutron dark decay model [8, 9] and in a quark vector current portal framework [10, 11].

The neutron dark decay model finds its origin in the recent neutron lifetime anomaly which is a $\sim 4\sigma$ discrepancy [12] in the neutron lifetimes measured in beam [13, 14] and bottle [15–17] experiments. If the neutron has the dark decay, $n \to \chi + \phi$, where χ and ϕ are dark sector particles, with a partial width of about 7.1×10^{-30} GeV the discrepancy is alleviated. The scalar ϕ is almost massless and no heavier than an MeV. The DM particle is very slightly lighter than the neutron and is a Dirac fermion to avoid constraints from neutron-antineutron oscillations. Multi-pion signatures in neutron-antineutron oscillation searches by Super-Kamiokande only constrain the model if the DM is $\bar{\chi}$ [18]. The model is interesting in that, as we will see, a NS can be composed of a substantial DM population, so that the DM capture rate can reach the geometric limit through DM self-interactions even if the DM-neutron scattering cross section is small.

As a second example, we consider dark matter that couples to u, d, s quarks through a dimensional-6 vector portal with independent couplings $\alpha_{u,d,s}$. These couplings can be chosen so that the DM capture rate reaches the geometric limit. The NS also gets heated by the annihilation of GeV DM to light mesons (which can be described by chiral perturbation theory [10, 11]).

The paper is organized as follows. In section 2, we review the process of DM capture by a NS, and the resultant NS temperature evolution is described in section 3. We study the neutron dark decay model in section 4, and the quark vector current portal model in section 5. We summarize our results in section 6.

2 Dark matter capture in neutron stars

DM capture by a NS is primarily governed by DM-nucleon scattering and by DM self-interactions if a significant DM population is bound by the NS. For weak scale DM, there are stringent upper limits on the DM-nucleon cross section, but constraints on DM self-interactions are relatively loose. Interestingly, the preferred range for the self-interaction cross section to alleviate the core-cusp problem is 0.1 cm^2/g $\lesssim \sigma_{\chi\chi}/m_\chi \lesssim 1$ cm^2/g [19]. This corresponds to $\sigma_{\chi\chi} \simeq 10^{-24} \frac{m_\chi}{1\text{ GeV}}$ cm^2, which is much weaker than the upper limit $\sigma_{\chi-\text{nucleon}} \lesssim 10^{-38}$ cm^2 from DM direct detection experiments [20]. Therefore, DM self-interactions may dramatically enhance the capture rate. Other processes, like DM-neutron annihilation, $\chi\bar{\chi}$ annihilation and neutron decays to DM, also affect DM capture, and

JHEP07(2020)181

Velocity dispersion of DM	$\bar{v} = 270$ km/s
Local DM density	$\rho_{\rm DM} = 0.4$ GeV/cm^3
NS velocity relative to GC	$v_N = 220$ km/s
NS mass	$M = 1.44 M_\odot = 2.86 \times 10^{33}$ g
NS radius	$R = 10.6$ km
NS fermion density	$\rho_F = 5.7 \times 10^{14}$ g/cm^3
NS fermion number density	$n_F = 3.4 \times 10^{38}$ cm^{-3} $= 2.125\, n_0$

Table 1. Parameter values for the DM halo and NS.

are included in our discussion below which is tailored for the neutron dark decay model; the corresponding equations for the quark vector current portal scenario are simpler and obtainable by straightforward modifications.

Because we study scenarios of Dirac fermion DM, the DM particle is either χ or $\bar{\chi}$. We consider the general case in which the NS is composed of both neutrons and χ, as is the case for the neutron dark decay model we consider. The evolution of the number of DM particles $N_{\rm DM}$ in the neutron star is described by [21]

$$\frac{dN_{\rm DM}}{dt} = \begin{cases} C_c + C_s^{\chi\chi}(N_{\rm DM} + N_\chi)\,, & \text{if DM is } \chi \\ C_c + (C_s^{\bar{\chi}\bar{\chi}} N_{\rm DM} + C_s^{\bar{\chi}\chi} N_\chi) - C_a^{\bar{\chi}n} N_{\rm DM} N_n - C_a N_{\rm DM} N_\chi\,, & \text{if DM is } \bar{\chi} \end{cases} \tag{2.1}$$

where we distinguish the component N_χ produced by neutron decay, $n \to \chi + \phi$, from the halo DM component $N_{\rm DM}$ because they may have different thermal properties. We assume that the rate of $n \to \chi + \phi$ is large enough to keep the neutrons and χ in thermal equilibrium. Halo DM-neutron elastic scattering contributes to the capture rate, and if DM is $\bar{\chi}$, halo DM also annihilates with neutrons, which under the assumption of a uniform mass distribution, are respectively given by [1]

$$\begin{aligned} C_c &= \sqrt{\frac{6}{\pi}} \frac{\rho_{\rm DM}}{m_\chi} \frac{v_{\rm esc}^2(R)}{\bar{v}^2} (\bar{v} \xi \sigma_{{\rm DM}-n}^{\rm elastic}) N_n \left(1 - \frac{1 - e^{-B^2}}{B^2}\right)\,, \\ C^{\rm ann} &= \sqrt{\frac{6}{\pi}} \frac{\rho_{\rm DM}}{m_\chi} \frac{v_{\rm esc}^2(R)}{\bar{v}^2} (\bar{v} \sigma_{\bar{\chi}n}^{\rm ann}) N_n \left(1 - \frac{1 - e^{-B^2}}{B^2}\right)\,, \end{aligned} \tag{2.2}$$

where the escape velocity of the NS is $v_{\rm esc}(R) = \sqrt{2GM/R} \simeq 0.63\, c$, $\bar{v}$ is the DM dispersion velocity, and $\rho_{\rm DM}$ is the local DM density; the relevant parameter values for the NS and the DM halo are listed in table 1. N_n is the total number of neutrons in the NS, and $B^2 \equiv (3/2)(v_{\rm esc}^2/\bar{v}^2)\beta_-$ with $\beta_- = 4 m_\chi m_n/(m_\chi - m_n)^2$ appears after averaging over the DM velocity distribution. Of course, $m_{\rm DM} \equiv m_\chi = m_{\bar{\chi}}$.

We assume that the neutrons inside the NS behave as a Fermi gas and estimate the Fermi momentum to be $p_F \simeq (3\pi^2 \rho_F/m_n)^{1/3} = 437\,{\rm MeV}$. DM-neutron scattering only occurs when the momentum exchange δp is larger than p_F. We take this Pauli blocking into account by introducing a factor $\xi = \min(\delta p/p_F, 1)$ in the above capture rate C_s. Note that once the sum of cross sections ($\xi \sigma_{\chi n}^{\rm elastic}$ for χ DM, or $\xi \sigma_{\bar{\chi}n}^{\rm elastic} + \sigma_{\bar{\chi}n}^{\rm ann}$ for $\bar{\chi}$ DM) is

JHEP07(2020)181

larger than critical cross section, $\sigma_{\rm crit} = \pi R^2 m_n/M$, and the sum of the capture rate and annihilation rates cannot be larger than the geometric limit, i.e., $C_c + C^{\rm ann} \leq C_c|_{\rm geom}$. This is equivalent to $N_n(\xi\sigma^{\rm elastic}_{\chi n}) \leq \pi R^2$ if DM is χ, and $N_n(\xi\sigma^{\rm elastic}_{\bar\chi n} + \sigma^{\rm ann}_{\bar\chi n}) \leq \pi R^2$ if DM is $\bar\chi$. For 1 GeV χ DM, the geometric limit $C_c|_{\rm geom} \simeq 8.2\times10^{32}\,{\rm yr}^{-1}$ corresponds to $\sigma_{\rm crit} \simeq 10^{-45}$ cm^2 [5].

The DM capture rate due to scattering on χ from neutron conversion inside the NS or on the trapped DM (whose population is negligible in comparison) is [2]

$$C_s^{\chi\chi} = C_s^{\bar\chi\bar\chi} = \sqrt{\frac{3}{2}}\frac{\rho_{\rm DM}}{m_\chi}\sigma_{\chi\chi\to\chi\chi}v_{\rm esc}(R)\frac{v_{\rm esc}(R)}{\bar v}\frac{{\rm erf}(\eta)}{\eta}\frac{1}{1-\frac{2GM}{R}}\,,$$
$$C_s^{\bar\chi\chi} = \sqrt{\frac{3}{2}}\frac{\rho_{\rm DM}}{m_\chi}\sigma_{\bar\chi\chi\to\bar\chi\chi}v_{\rm esc}(R)\frac{v_{\rm esc}(R)}{\bar v}\frac{{\rm erf}(\eta)}{\eta}\frac{1}{1-\frac{2GM}{R}}\,, \tag{2.3}$$

where we have again assumed that the mass density of the NS is uniform. Here, $\eta = \sqrt{3/2}(v_N/\bar v)$, with v_N the NS velocity relative to the Galactic center. For these cases, we define the geometric limits, $N_\chi\sigma_{\chi\chi\to\chi\chi} \leq \pi R^2$ and $N_\chi\sigma_{\bar\chi\chi\to\bar\chi\chi} \leq \pi R^2$. The trapped DM with velocity $v_{\rm DM}$ will form its own sphere of radius $r_{\rm DM}(t)$, and the evolution of $r_{\rm DM}(t)$ is derived as follows. The kinetic energy of each DM particle can be expressed in terms of the orbital radius $r_{\rm DM}(t)$ as [2]

$$E_{\rm DM} = \frac{2\pi}{3}G\rho_F m_\chi r_{\rm DM}^2 = \frac{1}{2}m_\chi v_{\rm DM}^2\,, \tag{2.4}$$

with the rate of change in kinetic energy given by [1]

$$\frac{dE_{\rm DM}}{dt} = \begin{cases} -\xi'\left[n_F(1-a_\chi)\sigma^{\rm elastic}_{\chi n} + n_F a_\chi\sigma_{\chi\chi\to\chi\chi}\right]v_{\rm DM}\delta E\cdot{\rm sign}(T_{\rm DM}-T_{\rm int}) & \\ +\,C_s^{\chi\chi}\Delta E\,, & \text{if DM is } \chi \\ -\xi'\left[n_F(1-a_\chi)\sigma^{\rm elastic}_{\bar\chi n} + n_F a_\chi\sigma_{\bar\chi\chi\to\bar\chi\chi}\right]v_{\rm DM}\delta E\cdot{\rm sign}(T_{\rm DM}-T_{\rm int}) & \\ +\,C_s^{\bar\chi\bar\chi}\Delta E\,, & \text{if DM is } \bar\chi \end{cases} \tag{2.5}$$

where a_χ is the fractional number of χ in the NS, and $1-a_\chi$ is the fractional number of neutrons in the NS. The first (second) term in brackets corresponds to an energy release $\delta E = 2m_r E_{\rm DM}/(m_n+m_\chi)$ to the neutron component (χ component) of the NS [2], where m_r is the reduced mass of the DM-neutron system.[1] The energy gain, $\Delta E = \frac{1}{2}m_\chi(v_{\rm esc}^2 - v_{\rm DM}^2)$, results from a drop in the halo DM's potential energy from $\frac{1}{2}m_\chi v_{\rm esc}^2$ to $\frac{1}{2}m_\chi v_{\rm DM}^2$ after thermalizing with the trapped DM. Here,

$$\frac{1}{2}m_\chi v_{\rm esc}^2 = \frac{GMm_\chi}{R} + \frac{GMm_\chi}{R^3}\left(\frac{R^2 - r_{\rm DM}^2}{2}\right)\,.$$

Effects of Pauli blocking are included by the factor, $\xi' = \min(\sqrt{2}m_r v_{\rm DM}/p_F, 1)$. The evolution of $r_{\rm DM}(t)$ is obtained by combining eqs. (2.4) and (2.5), and the temperature of the DM sphere $T_{\rm DM}$ is given by $\frac{3}{2}kT_{\rm DM}(t) = E_{\rm DM}$.

[1] The analytic expression for δE is a valid approximation only if the DM particle is much more energetic than the neutron, and $m_\chi \sim m_n$ [2]. Equation (2.5) is used to determine if the trapped DM and neutron can achieve thermal equilibrium, a condition that is easily satisfied in the neutron dark decay model. Therefore, this approximation has little effect on our results.

JHEP07(2020)181

The last two terms in the second equation in eq. (2.1) depends on the DM-neutron and DM-antiDM annihilation rates [21]

$$C_a^{\bar{\chi}n} \simeq \frac{\langle \sigma^{\rm ann}_{\bar{\chi}n} v_{\rm DM} \rangle}{4\pi R^3/3}\,, \quad C_a \simeq \frac{\langle \sigma^{\rm ann}_{\bar{\chi}\chi} v_{\rm DM} \rangle}{4\pi R^3/3}\,, \tag{2.6}$$

which depletes the total number of trapped DM.

3 Temperature evolution

Soon after a NS is formed in a supernova explosion, its core has a temperature of about 10^{11} K. It then cools down to 10^8 K through neutrino emission in about 10^5 years. When the core temperature falls below 10^8 K, photon emission dominates the cooling process. Unlike neutrino cooling, whose detailed mechanism is still under debate, photo cooling has less uncertainty, and we focus on this period of a neutron star's life.

The interior temperature $T_{\rm int}$ of a NS evolves according to [4]

$$\frac{dT_{\rm int}}{dt} = \frac{-\epsilon_\nu - \epsilon_\gamma + \epsilon_{\rm DM}}{c_V}\,, \tag{3.1}$$

where $\epsilon_{\nu,\gamma,{\rm DM}}$ are the neutrino, photon and DM emissivities, and c_V is the NS heat capacity per unit volume. Treating neutrons and the χ from neutron conversion as ideal Fermi gases, c_V is given by [22, 23]

$$c_V = \frac{k_B^2 T_{\rm int}}{3} \sum_{i=\chi,n} p_{F,i} \sqrt{m_i^2 + p_{F,i}^2}\,, \tag{3.2}$$

where the Fermi momenta are

$$\begin{aligned} p_{F,\chi} &= 0.34 \text{ GeV} \left(\frac{n_F a_\chi}{n_0}\right)^{1/3}\,, \\ p_{F,n} &= 0.34 \text{ GeV} \left(\frac{n_F (1-a_\chi)}{n_0}\right)^{1/3}\,. \end{aligned} \tag{3.3}$$

The neutrino emissivity is [22, 23]

$$\epsilon_\nu \simeq 1.81 \times 10^{-27} \text{ GeV}^4 \text{yr}^{-1} \left(\frac{n_F}{n_0}\right)^{2/3} \left(\frac{T_{\rm int}}{10^7 \text{ K}}\right)^8\,,$$

where $n_0 = 0.16 \text{ fm}^{-3} = 0.16 \times 10^{39} \text{ cm}^3$, and n_F is the average fermion number density in a NS.[2] Since neutrino emission depends on the eighth power of $T_{\rm int}$, neutrinos easily escape the NS when it is young. The surface temperature $T_{\rm sur}$ of a NS is related to $T_{\rm int}$ via [24–26]

$$T_{\rm sur} = \begin{cases} 0.87 \times 10^6 \text{ K} \left(\frac{g_s}{10^{14} \text{ cm s}^{-2}}\right)^{1/4} \left(\frac{T_{\rm int}}{10^8 \text{ K}}\right)^{0.55}\,, & T_{\rm int} \gtrsim 3700 \text{ K} \\ T_{\rm int}\,, & T_{\rm int} \lesssim 3700 \text{ K} \end{cases} \tag{3.4}$$

[2] Since the neutron radius is ~ 1 fm, n_0 sets the scale for the critical density of a NS. A NS with central density of $6n_0$ has a $\sim 2M_\odot$ mass which depends on the nuclear equation of state.

JHEP07(2020)181

where $g_s = GM/R^2 = 1.85 \times 10^{14}\ \mathrm{cm\,s^{-2}}$ is the gravitational acceleration at the surface of the NS. Including the effect of gravitational redshift, the observed temperature $T_{\rm obs}$ at infinity is [27]

$$T_{\rm obs} = T_{\rm sur}\sqrt{1 - \frac{2GM}{Rc^2}}\,.$$

The NS luminosity L_γ from the outer envelope is given by the Stefan-Boltzmann law:

$$L_\gamma = 4\pi R^2 \sigma_{\rm SB} T_{\rm sur}^4 \simeq 5.00 \times 10^{11}\ \mathrm{GeV\,s^{-1}} \left(\frac{T_{\rm sur}}{\rm K}\right)^4\,, \tag{3.5}$$

where $\sigma_{\rm SB} = 3.5383 \times 10^{-2}\ \mathrm{GeV\,cm^{-2}\,s^{-1}\,K^{-4}}$ is the Stefan-Boltzmann constant. Then the effective photon emissivity is

$$\epsilon_\gamma = \frac{L_\gamma}{4\pi R^3/3} \simeq \begin{cases} 2.59 \times 10^{-17}\ \mathrm{GeV^4\,yr^{-1}} \left(\frac{T_{\rm int}}{10^8\ \rm K}\right)^{2.2}\,, & T_{\rm int} \gtrsim 3700\ \mathrm{K} \\ 2.44 \times 10^{-9}\ \mathrm{GeV^4\,yr^{-1}} \left(\frac{T_{\rm int}}{10^8\ \rm K}\right)^{4}\,, & T_{\rm int} \lesssim 3700\ \mathrm{K}\,. \end{cases}$$

Photon emission dominates the cooling process after 10^5 years, when $T_{\rm obs} \lesssim 10^6$ K.

Dark matter can inject energy into a NS in several ways. Halo DM-neutron elastic scattering and halo DM-neutron annihilation (if the DM is $\bar\chi$) contribute energy,

$$\mathcal{K}_{\rm DM} = \begin{cases} C_c \langle E_R\rangle\,, & \text{if DM is } \chi \\ C_c \langle E_R\rangle + C^{\rm ann}\,(m_\chi + m_n)\,, & \text{if DM is } \bar\chi \end{cases}$$

where

$$\langle E_R\rangle \equiv \frac{\int_{-1}^{1} d\cos\theta_{\rm cm}\, E_R \frac{d\sigma_{{\rm DM}-n}}{d\cos\theta_{\rm cm}}}{\int_{-1}^{1} d\cos\theta_{\rm cm} \frac{d\sigma_{{\rm DM}-n}}{d\cos\theta_{\rm cm}}} \simeq \frac{(1-\bar B) m_\chi \bar\mu}{\bar B + 2\sqrt{\bar B}\bar\mu + \bar B \bar\mu^2}\,,$$

is the angular average recoil energy transferred from the DM to a neutron in a single collision [27]. Here, $\bar B \equiv 1 - 2GM/(c^2 R) \simeq 0.60$ and $\bar\mu \equiv m_\chi/m_n$. For $m_\chi \simeq m_n$ we find $\langle E_R\rangle \simeq 0.15 m_\chi$, which implies that annihilation is more efficient than elastic scattering at heating a NS if the halo DM-neutron annihilation and elastic scattering rates are comparable.

Another source of heat is the annihilation of trapped DM. If the trapped DM is $\bar\chi$, it can annihilate with χ from neutron conversion or with neutrons into SM particles and inject energy,

$$\mathcal{E}_{\rm DM} = \begin{cases} 0\,, & \text{if DM is } \chi \\ 2 m_\chi C_a N_{\rm DM} N_\chi f_{\rm DM} + (m_n + m_\chi) C_a^{\bar\chi n} N_{\rm DM} N_n\,, & \text{if DM is } \bar\chi \end{cases}$$

where $f_{\rm DM} \subset [0,1]$ is the efficiency with which energy is absorbed by the NS and depends on the annihilation final states. For instance, $f_{\rm DM} = 0$ for a purely neutrino final state, and $f_{\rm DM} = 1$ for a $\gamma\gamma$ final state. In principle, the contribution from $\bar\chi$-neutron annihilation also has an efficiency factor, but we approximate this to unity for the final states we consider later; this also applies to the annihilation term in $\mathcal{K}_{\rm DM}$ above.

JHEP07(2020)181

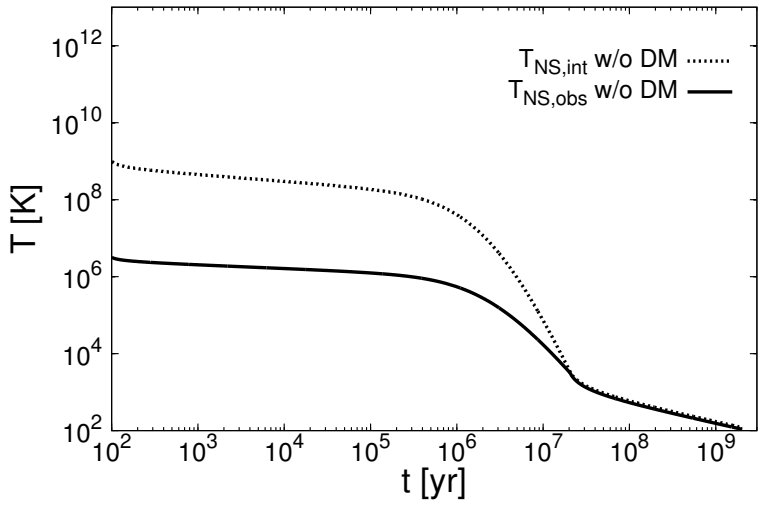

Figure 1. The time evolution of the interior and observed NS temperatures without DM capture.

The trapped DM also releases its energy via elastic scattering with neutrons and with χ from neutron conversion:

$$\mathcal{F}_{\rm DM} = \begin{cases} \xi' \left[n_F (1-a_\chi) \sigma_{\chi n}^{\rm elastic} + n_F a_\chi \sigma_{\chi\chi\to\chi\chi} \right] v_{\rm DM} \delta E \, N_{\rm DM} \cdot {\rm sign}(T_{\rm DM} - T_{\rm int}), & \text{if DM is } \chi \\ \xi' \left[n_F (1-a_\chi) \sigma_{\bar\chi n}^{\rm elastic} + n_F a_\chi \sigma_{\bar\chi\chi\to\bar\chi\chi} \right] v_{\rm DM} \delta E \, N_{\rm DM} \cdot {\rm sign}(T_{\rm DM} - T_{\rm int}), & \text{if DM is } \bar\chi \end{cases} . \tag{3.6}$$

From eqs. (2.5) and (3.6), we see the path of energy conduction. The kinetic energy lost by halo DM to become trapped is transferred to the NS through scattering processes.

Summing over the above three contributions, the total DM emissivity is

$$\epsilon_{\rm DM} = \frac{\mathcal{K}_{\rm DM} + \mathcal{E}_{\rm DM} + \mathcal{F}_{\rm DM}}{4\pi R^3/3} . \tag{3.7}$$

The time evolution of the interior and observed temperatures of a NS without DM heating are shown in figure 1. For an old NS of age between 10^8 and 10^9 years, the temperature falls to about 500 K and 150 K, respectively.

In the rest of this section we do not consider the possibility of neutron conversion to χ and DM-neutron annihilation. Neutron star heating by DM capture can compensate the cooling from photon emission once $T_{\rm int}$ falls to ~ 1000 K. The NS can be heated by two processes: *i*) kinetic heating by the captured DM, and *ii*) DM annihilation into SM final states.

In the case of kinetic heating, if the capture rate is at the geometric limit, the observed (surface) temperature increases to 1480 (1660) K after the photon emission and DM kinetic heating processes attain equilibrium, $L_\gamma|_{T_{\rm sur}=1660\,{\rm K}} = C_c|_{\rm geom}\langle E_R\rangle$. The left panel of figure 2 shows that $T_{\rm obs}$ flattens out at 1480 K after 5×10^7 yrs.

DM annihilation consumes the entire DM mass to heat up the NS, and if the annihilation rate is high enough, photon emission and DM heating reach equilibrium earlier.

JHEP07(2020)181

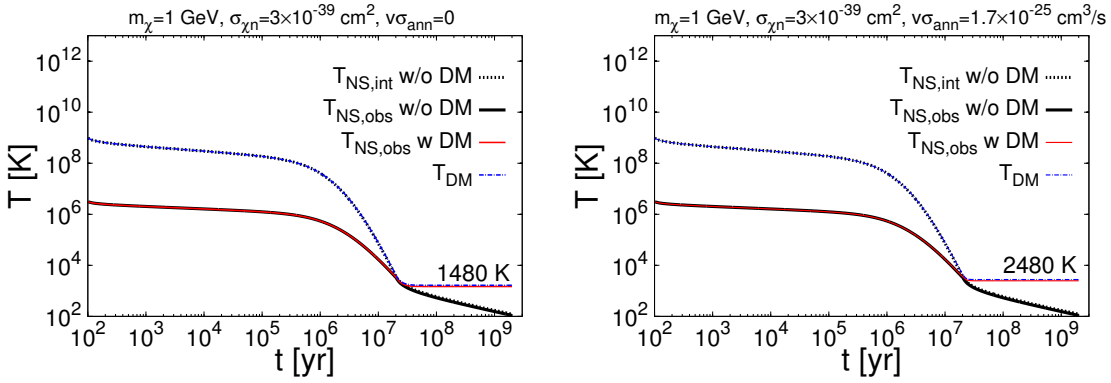

Figure 2. The time evolution of NS temperatures including DM heating. The left panel does not have a contribution from DM annihilation, and the right panel does.

The observed (surface) temperature increases to 2480 (2780) K, when the photon emission energy-loss rate equals the sum of the DM kinetic and annihilation heating rate: $L_\gamma|_{T_{\rm sur}=2780\,{\rm K}} = C_c|_{\rm geom}(\langle E_R\rangle + m_\chi)$; see the right panel of figure 2. The surface temperature $T_{\rm sur}$ saturates at 2780 K, when the DM annihilation rate equals the DM capture rate, i.e., $N_{\rm DM}^2 C_a|_{\rm sat} \simeq C_c$. Estimating $N_{\rm DM}$ by multiplying $C_c = C_c|_{\rm geom}$ with the typical age of an old NS, 5×10^8 yr, we find the saturating DM annihilation cross section to be $v_{\rm DM}\sigma^{\rm ann}_{\bar\chi\chi}|_{\rm sat} \simeq 10^{-39}\,{\rm cm}^3/{\rm s}$. Clearly, increasing $v_{\rm DM}\sigma^{\rm ann}_{\bar\chi\chi}$ above $v_{\rm DM}\sigma^{\rm ann}_{\bar\chi\chi}|_{\rm sat}$ does not increase $T_{\rm obs}$.

In general, the value of $v_{\rm DM}\sigma^{\rm ann}_{\bar\chi\chi}|_{\rm sat}$ depends on C_c and $\sigma^{\rm elastic}_{{\rm DM}-n}$. For example, consider a smaller capture rate, $C_c = 10^{-4}\times C_c|_{\rm geom}$. Without the heating from DM annihilation, the equilibrium condition, $L_\gamma|_{T_{\rm sur}=170\,{\rm K}} = C_c\langle E_R\rangle$, gives a final NS surface temperature $T_{\rm sur} = 170\,{\rm K}$. Including DM annihilation increases the surface temperature to $T_{\rm sur} = 280\,{\rm K}$ using the criterion, $L_\gamma|_{T_{\rm sur}=280\,{\rm K}} = C_c(\langle E_R\rangle + m_\chi)$. In this case, $v_{\rm DM}\sigma^{\rm ann}_{\bar\chi\chi}|_{\rm sat} \simeq 10^{-35}\,{\rm cm}^3/{\rm s}$.

In the neutron dark decay model, the trapped DM $\bar\chi$ can annihilate with the neutron or χ from neutron conversion to provide additional heating. The observed (surface) temperature can reach 3100 (3440) K, if the photon emission energy-loss rate equals the sum of the DM kinetic and annihilation heating rates: $L_\gamma|_{T_{\rm sur}=3440\,{\rm K}} = C_c|_{\rm geom}(\langle E_R\rangle + 2m_\chi)$.

4 Neutron dark decay model

The defining feature of the neutron dark decay model is that the neutron decays to dark sector particles χ and ϕ. In the low energy limit, this can be described as a mixing between the neutron and the Dirac particle χ, which could serve as DM. However, since the DM particle is a Dirac fermion, either χ or $\bar\chi$ could be DM, with different interactions with the neutron. Only $\bar\chi$ can annihilate with the neutron, and only χ is produced from neutron conversion. We separately discuss the phenomenologies of NS heating for these two cases.

4.1 Model and NS equation of state

The interaction terms in the model are [8, 9]

$$\mathcal{L} \supset \lambda_q \epsilon^{ijk}\bar u^c_{Li} d_{Rj}\Phi_k + \lambda_\chi \Phi^{*i}\bar{\tilde\chi} d_{Ri} + \lambda_\phi \bar{\tilde\chi}\chi\phi + \mu H^\dagger H\phi + g_\chi\bar\chi\chi\phi + {\rm h.c.}\,, \tag{4.1}$$

JHEP07(2020)181

where the heavy scalar $\Phi = (3,1)_{-1/3}$ (color triplet, weak singlet, hypercharge -1/3) has mass above a TeV, and two Dirac fermions $\tilde{\chi}$ and χ, and a scalar ϕ, are SM singlets The baryon number assignments for $\Phi, \tilde{\chi}, \chi, \phi$ are $-2/3, 1, 1, 0$, respectively.[3] The annihilation process $\bar{\chi}\chi \to \phi\phi$ produces the observed DM relic abundance if the coupling $\lambda_\phi \simeq 0.04$. The first three interaction terms allow the decay $n \to \chi\phi$, which makes the NS unstable [31]. Including the Higgs portal and the $g_\chi \bar{\chi}\chi\phi$ coupling, induces a repulsive χ-neutron interaction, which causes the energy density to increase when converting a neutron into χ, so that the neutron becomes stable inside a NS [9]. Then the interaction $g_n \bar{n} n \phi$ is generated from the Higgs portal interaction through the pion with

$$g_n = \frac{\mu \sigma_{\pi n}}{m_h^2}\,, \tag{4.2}$$

where $\sigma_{\pi n} = 370\,\text{MeV}$ and Higgs mass $m_h = 125\,\text{GeV}$.

Constraints from rapid red giant star cooling [32] require $|g_n| \lesssim 10^{-14}$. The sufficient condition to stabilize the NS is [9]

$$z \equiv \frac{m_\phi}{\sqrt{|g_\chi g_n|}} \lesssim 71\ \text{MeV}\,, \tag{4.3}$$

which puts the NS in the neutron phase, and no χ is produced. Then the NS mass can reach two solar masses with central density of $6n_0$. For very light ϕ, the choice, $m_\phi \simeq 0.1$ eV, $g_\chi \simeq 4 \times 10^{-4}$, and $\mu \simeq -0.4$ eV, gives $z \simeq 50\,\text{MeV}$ to stabilize the NS, and also provides DM self-scattering cross sections of $0.1\ \text{cm}^2/\text{g} \lesssim \sigma/m_\chi \lesssim 1\ \text{cm}^2/\text{g}$ which alleviates the tension between N-body simulations of collisionless cold DM and large scale structure observations [9]. However, if $m_\phi > 13\,\text{eV}$, $g_n = -10^{-14}$, and $g_\chi \lesssim \sqrt{4\pi}$, z can easily exceed 71 MeV. Therefore, for heavier ϕ, the NS is in a mixed phase, and we must solve the equation of state (EoS) equation to obtain the number densities, n_χ and n_n in the NS. In the mixed phase, the NS can be stabilized by introducing a repulsive DM self-interaction, and achieve a NS mass of about $2M_\odot$.

We solve the EoS equation as follows. The energy density in a NS in a mixed phase is [9]

$$\varepsilon(n_n, n_\chi) = \varepsilon_{\text{nuc}}(n_n) + \varepsilon_\chi(n_\chi) + \frac{n_\chi n_n}{2z^2}\,, \tag{4.4}$$

where we assume χ is an ideal Fermi gas, and neutrons follow the EoS labeled $V_{3\pi} + V_R$ in ref. [33], corresponding to moderately stiff EoSs that incorporate 3-nucleon forces and have been fit to the results of a quantum Monte Carlo. Then,

$$\begin{aligned} \varepsilon_\chi &= \frac{m_\chi^4}{8\pi^2}\left[x\sqrt{1+x^2}(1+2x^2) - \ln(x+\sqrt{1+x^2})\right] \pm \frac{n_\chi^2}{2z'^2}\,, \qquad x \equiv \frac{(3\pi^2 n_\chi)^{1/3}}{m_\chi}\,, \\ \varepsilon_{\text{nuc}} &= a x'^\alpha + b x'^\beta\,, \qquad\qquad\qquad\qquad\qquad\qquad\qquad\qquad x' \equiv \frac{n_n}{n_0} \end{aligned} \tag{4.5}$$

[3] The asymmetry between χ and $\bar{\chi}$ may originate as in models of asymmetric dark matter [28, 29]. Since χ has the same baryon number as the neutron, chemical equilibrium in the early universe may relate the DM asymmetry to the baryon asymmetry. In asymmetric dark matter models, the DM particle has a GeV mass to reproduce the observed relic abundance.

JHEP07(2020)181

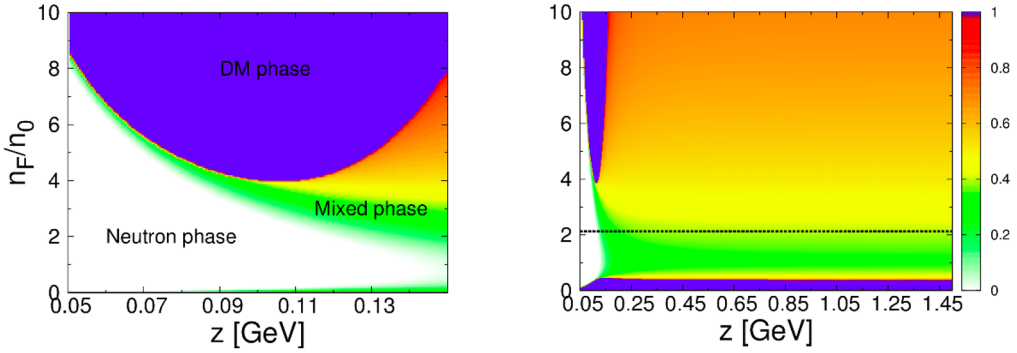

Figure 3. The three phases of the NS. The right panel shows n_F/n_0 for a wider range in z. The shading indicates n_χ/n_F for a given n_F. For the NS we consider, $n_F \simeq 2.125\, n_0$, which is indicated by the dashed horizontal line. In this case χ contributes about 40% of the total number density of the NS.

with $a\,(b) = 13.0\,(3.21)\,\mathrm{MeV}$, $\alpha\,(\beta) = 0.49\,(2.47)$ [34]. Here, $z' \equiv m_\phi/g_\chi$ comes from the DM self-interaction, which if mediated by a scalar or vector boson results in an attractive or repulsive force, respectively. A repulsive DM self-interaction can be realized by introducing an additional vector boson into the model; see ref. [34] for details on the model construction. Here, we simply fix the ratio of $z/z' = \sqrt{|g_\chi|/|g_n|} \simeq 2 \times 10^5$, although in general, z and z' are two independent parameters. The equilibrium condition is

$$0 = \frac{\partial \varepsilon(n_F - n_\chi, n_\chi)}{\partial n_\chi} = \mu_\chi(n_\chi) - \mu_{\mathrm{nuc}}(n_n) + \frac{n_F - 2n_\chi}{2z^2}\,, \tag{4.6}$$

which is used to determine the n and χ compositions of the NS. The total Fermion number density satisfies $n_F = n_n + n_\chi$. The neutron phase is determined by the condition $\partial\varepsilon/\partial n_\chi|_{n_\chi=0} > 0$, which requires that no χ be present, because introducing one χ increases the energy density. On the other hand, the condition $\partial\varepsilon/\partial n_\chi|_{n_\chi=n_F} < 0$, transforms the entire NS into a χ star. The mixed phase is defined by $\partial\varepsilon/\partial n_\chi|_{0<n_\chi<n_F} = 0$. The three phases are shown in the left panel of figure 3 in the $(z, n_F/n_0)$ plane. The shading shows the density ratio $a_\chi \equiv n_\chi/(n_n + n_\chi)$, which is almost independent of z for $z \gtrsim 0.25\,\mathrm{GeV}$. The minimal composition of χ occurs for $n_F \simeq n_0$, in which case χ contributes about 30% of the total number density.

The scenario with DM self-interactions is shown in figure 4. The lower panel corresponds to repulsive DM self-interactions which helps to stabilize the neutron star and extends the neutron phase up to $z \simeq 10^3\,\mathrm{GeV}$. We also solve the Tolman-Oppenheimer-Volkoff equation [35] to check that neutron stars heavier than $2M_\odot$ are obtainable. From the correlation between total pressure $P = n_F^2 d(\varepsilon/n_F)/dn_F$ and ε, we find the relations between the NS mass and radius in figure 5. From the left and middle panels we see that once $z' \lesssim 100\,\mathrm{MeV}$, the NS mass can be larger than $2M_\odot$ for the repulsive case. It is noteworthy that the NS in the repulsive case in the middle panel is in a mixed phase, and can still reach $2M_\odot$.

JHEP07(2020)181

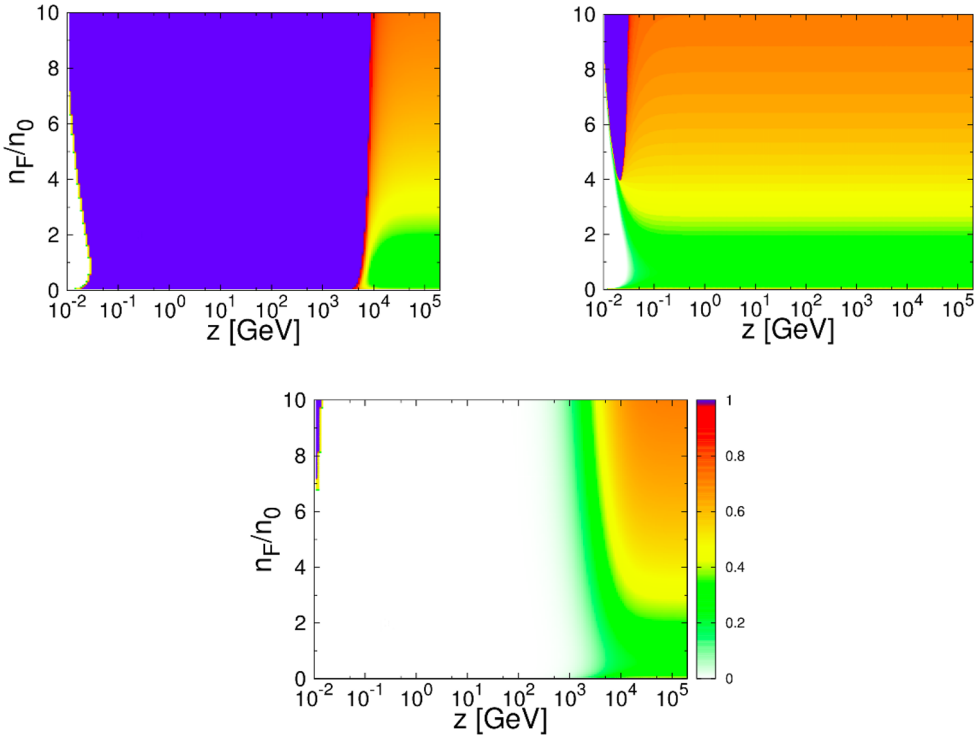

Figure 4. Same as figure 3, but including DM self-energy and for $z/z' \simeq 2 \times 10^5$. Upper-Left panel: attractive DM self-energy $-\frac{n_\chi^2}{2z'^2}$. Upper-Right panel: without DM self-energy. Low-middle panel: repulsive DM self-energy $+\frac{n_\chi^2}{2z'^2}$.

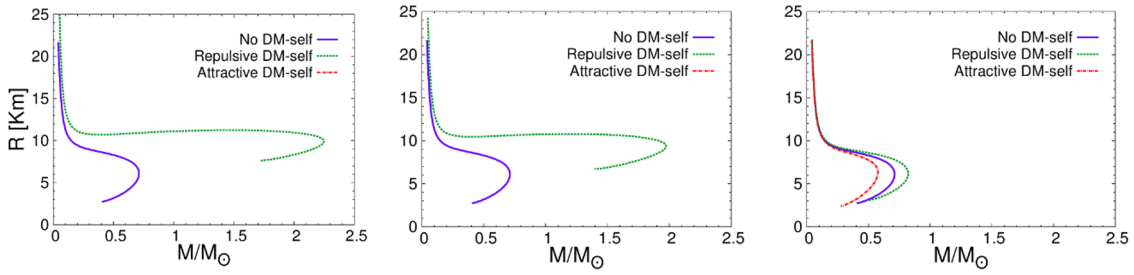

Figure 5. The NS mass for the neutron dark decay model for $z = 10^3, 10^4, 10^5$ GeV in the left, middle, right panels, respectively, with $z/z' \simeq 2 \times 10^5$.

4.2 DM-DM scattering cross section

The DM self-scattering cross section arises from the $g_\chi \bar{\chi}\chi\phi$ and $\lambda_\phi \bar{\tilde{\chi}}\chi\phi$ terms in the Lagrangian. The former is from the t-channel ϕ exchange diagram, while the later is generated from box diagrams with $\tilde{\chi}$ and ϕ in the loop. Since $\lambda_\phi \simeq 0.04$ is much larger than $g_\chi \simeq 4 \times 10^{-4}$, the loop-diagram contribution is comparable with the tree-level one. Since a large fraction of the NS could be composed of χ, DM self-capture is crucial for NS heating.

JHEP07(2020)181

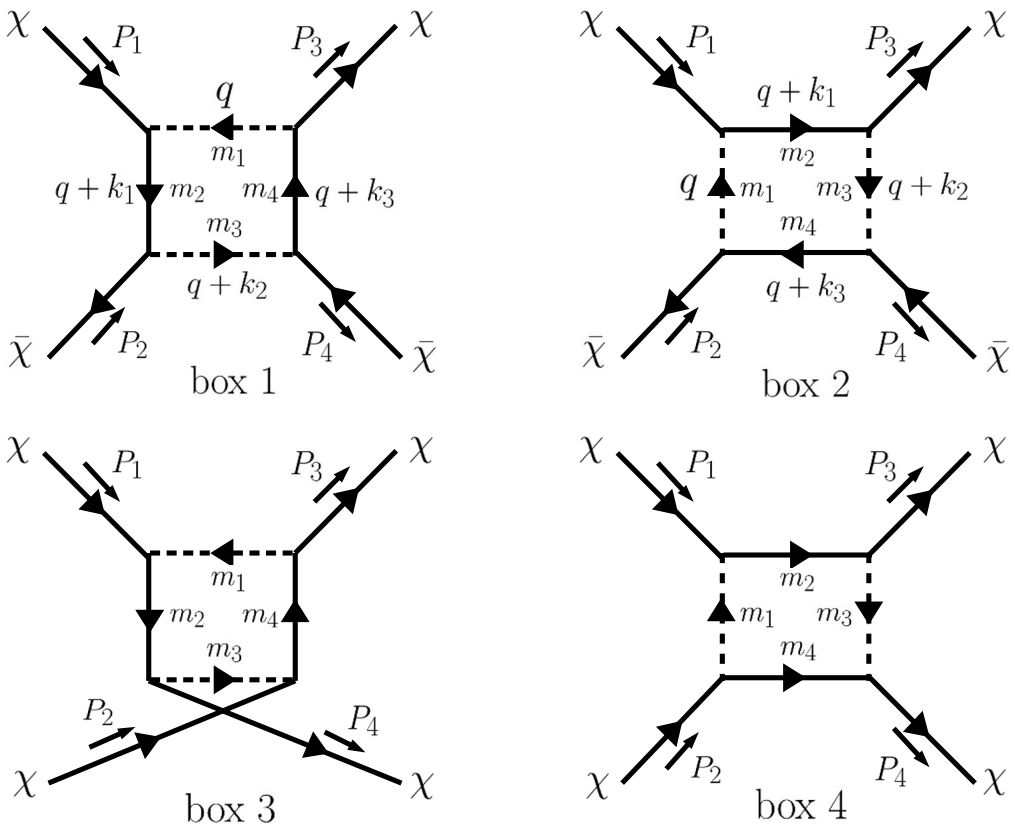

Figure 6. Box-1 and box-2 are for $\bar{\chi}\chi \to \bar{\chi}\chi$, while box-3 and box-4 are for $\chi\chi \to \chi\chi$, where $m_1 = m_3 = m_\phi$, $m_2 = m_4 = m_{\tilde{\chi}}$. In box-1, $k_1 = p_1$, $k_2 = p_1 + p_2$, $k_3 = p_3$, while in box-2, $k_1 = p_1$, $k_2 = p_1 - p_3$, $k_3 = -p_2$.

The DM self-scattering cross section due to the $g_\chi \bar{\chi}\chi\phi$ term has been calculated in ref. [19]. The velocity-dependent cross section, which is inversely related to the fourth power of the velocity, was proposed to solve the core-cusp problem. During DM capture by a NS the typical DM velocity reaches $v \simeq 0.63c$, which suppresses this cross section to $\sigma^{\rm eff}_{\chi\chi\to\chi\chi} \simeq 8.0 \times 10^{-40}$ cm^2. Thus, the DM self-scattering cross section from $g_\chi \bar{\chi}\chi$ becomes comparable to that from $\lambda_\phi \bar{\tilde{\chi}}\chi\phi$ (via box diagrams), as we discuss below.

The DM self-scattering diagrams from the $\lambda_\phi \bar{\tilde{\chi}}\chi\phi$ term, are shown in figure 6. The amplitudes for $\chi(p_1)\bar{\chi}(p_2) \to \chi(p_3)\bar{\chi}(p_4)$ from box-1 and box-2 of figure 6 are, respectively,

$$\begin{aligned} i\mathcal{M}_{\rm box-1} = (\lambda_\phi^4)\, \{ & [\bar{v}(p_2)\gamma_\mu u(p_1)][\bar{u}(p_3)\gamma_\nu v(p_4)] D^{\mu\nu} \\ & + (m_\chi + m_{\tilde{\chi}})[\bar{v}(p_2)\gamma_\mu u(p_1)][\bar{u}(p_3) v(p_4)] D^{\mu} \\ & + (m_\chi + m_{\tilde{\chi}})[\bar{v}(p_2) u(p_1)][\bar{u}(p_3)\gamma_\nu v(p_4)] D^{\nu} \\ & + (m_\chi + m_{\tilde{\chi}})^2 [\bar{v}(p_2) u(p_1)][\bar{u}(p_3) v(p_4)] D_0 \} \,, \end{aligned} \tag{4.7}$$

$$\begin{aligned} i\mathcal{M}_{\rm box-2} = -(\lambda_\phi^4)\, \{ & [\bar{v}(p_2)\gamma_\mu v(p_4)][\bar{u}(p_3)\gamma_\nu u(p_1)] D^{\mu\nu} \\ & + (m_\chi + m_{\tilde{\chi}})[\bar{v}(p_2)\gamma_\mu v(p_4)][\bar{u}(p_3) u(p_1)] D^{\mu} \\ & + (m_\chi + m_{\tilde{\chi}})[\bar{v}(p_2) v(p_4)][\bar{u}(p_3)\gamma_\nu u(p_1)] D^{\nu} \\ & + (m_\chi + m_{\tilde{\chi}})^2 [\bar{v}(p_2) v(p_4)][\bar{u}(p_3) u(p_1)] D_0 \} \,, \end{aligned} \tag{4.8}$$

JHEP07(2020)181

where the relative minus sign arises from Fermi statistics. $D^{\mu\nu}$, $D^{\mu,\nu}$ and D_0 are loop integration functions defined in *LoopTools* [36] as

$$
\begin{aligned}
D_0 &= \frac{\mu^{4-d}}{i\pi^{d/2}\gamma_\Gamma}\int dq^d \frac{1}{[q^2-m_1^2][(q+k_1)^2-m_2^2][(q+k_2)^2-m_3^2][(q+k_3)^2-m_4^2]}\,,\\
D^{\mu} &= \frac{\mu^{4-d}}{i\pi^{d/2}\gamma_\Gamma}\int dq^d \frac{q^\mu}{[q^2-m_1^2][(q+k_1)^2-m_2^2][(q+k_2)^2-m_3^2][(q+k_3)^2-m_4^2]}\,,\\
D^{\mu\nu} &= \frac{\mu^{4-d}}{i\pi^{d/2}\gamma_\Gamma}\int dq^d \frac{q^\mu q^\nu}{[q^2-m_1^2][(q+k_1)^2-m_2^2][(q+k_2)^2-m_3^2][(q+k_3)^2-m_4^2]}\,,
\end{aligned}
\tag{4.9}
$$

where $d = 4-2\varepsilon$, $\gamma_\Gamma \equiv \frac{\Gamma^2(1-\varepsilon)\Gamma(1+\varepsilon)}{\Gamma(1-2\varepsilon)}$, and μ is the renormalization scale. In order to match the Dirac spinors between box-1 and box-2, we use the Fierz transformation [37]

$$
w_4\bar{w}_3 = \frac{1}{4}\left[(\bar{w}_3 w_4)\mathbb{I} + (\bar{w}_3\gamma^\alpha w_4)\gamma_\alpha + \frac{1}{2}(\bar{w}_3\sigma^{\alpha\beta}w_4)\sigma_{\alpha\beta} - (\bar{w}_3\gamma^\alpha\gamma_5 w_4)\gamma_\alpha\gamma_5 + (\bar{w}_3\gamma_5 w_4)\gamma_5\right]\,,
\tag{4.10}
$$

where Dirac spinor w represents either the u or v spinors. Then the crossing operation, $p_2 \to -p_4$ and $p_4 \to -p_2$, yields the amplitude for the DM self-scattering cross section $\chi\chi \to \chi\chi$ from box-3 and box-4.

The box diagrams are significantly enhanced by the $D^{\mu\nu}$ loop function when the scattering angle in the centre of mass frame approaches $\theta_{\rm cm} \simeq 0$ or π. This is due to the nearly massless mediator ϕ. Fortunately, neither collinear nor head on scattering contribute to the DM captured by DM inside the NS because the net trapped DM number remains the same in both cases. The energy transfer in a DM-DM collision is given by [27]

$$
\frac{(1-\bar{B})m_\chi}{2\bar{B}+2\sqrt{\bar{B}}}(1-\cos\theta_{\rm cm})\,,
\tag{4.11}
$$

where $\bar{B} \equiv 1-2GM/(c^2R)$ for a NS of mass M and radius R. So, the collinear scattering ($\theta_{\rm cm} \simeq 0$) cannot slow down the incoming DM enough to be trapped by the NS. On the other hand, head on scattering $\theta_{\rm cm} \simeq \pi$ exchanges the momenta of the two initial DM particles such that the incoming DM particle gets trapped and the target particle gets kicked out of the NS.

We define an effective DM self-scattering cross section, which is relevant to the DM captured inside the NS:

$$
\sigma^{\rm eff}_{\chi\bar{\chi}\to\chi\bar{\chi}} \equiv \int_0^\pi d\theta_{\rm cm}\frac{d\sigma_{\chi\bar{\chi}\to\chi\bar{\chi}}}{d\theta_{\rm cm}}(1-\cos\theta_{\rm cm})(1+\cos\theta_{\rm cm})\,,
\tag{4.12}
$$

and similarly for $\chi\chi \to \chi\chi$. The $(1-\cos\theta_{\rm cm})$ and $(1+\cos\theta_{\rm cm})$ factors are included to suppress the phase space contributions from collinear and head-on scatterings, respectively [38]. These factors also cancel the infrared divergence in $d\sigma_{\chi\bar{\chi}\to\chi\bar{\chi}}/d\theta_{\rm cm}$ that originates from the exchange of the light mediator ϕ, thereby rendering $\sigma^{\rm eff}_{\chi\bar{\chi}\to\chi\bar{\chi}}$ finite. The cross sections in figure 7 are finite. The loop-level contribution from $\lambda_\phi\bar{\chi}\chi\phi$ is comparable with the tree-level contribution from $g_\chi\bar{\chi}\chi\phi$ because $\lambda_\phi \gg g_\chi$.

JHEP07(2020)181

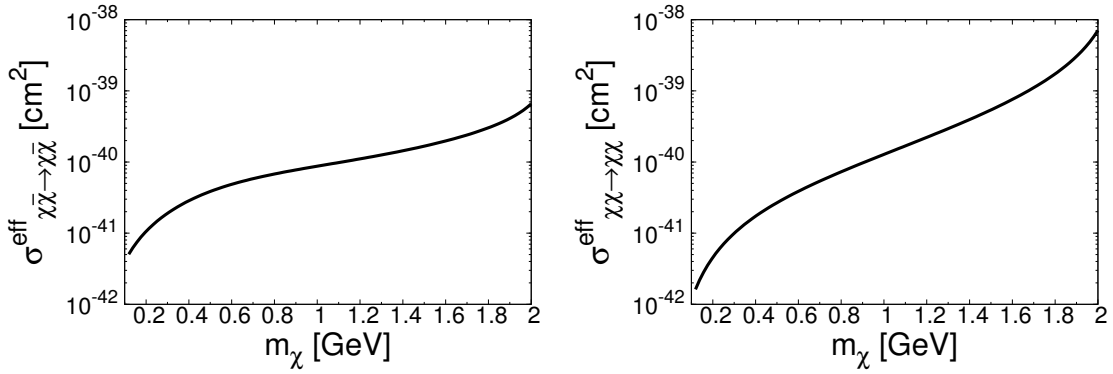

Figure 7. The cross sections $\sigma^{\rm eff}_{\chi\bar\chi\to\chi\bar\chi}$ and $\sigma^{\rm eff}_{\chi\chi\to\chi\chi}$ from the two box diagrams of figure 6. We set $\lambda_\phi = 0.04$, $m_{\tilde\chi} = 2\,\text{GeV}$, $m_\phi = 0.1\,\text{MeV}$.

4.3 DM-neutron elastic scattering and annihilation cross sections

At the GeV energy scale, the model can be described by an effective operator, $\mathcal{L} \supset \varepsilon(\bar n\tilde\chi + \bar{\tilde\chi} n)$, which mixes n and $\tilde\chi$ with mixing angle $\theta = \varepsilon/(m_n - m_{\tilde\chi})$. $\theta \simeq \mathcal{O}(10^{-11} - 10^{-12})$ accommodates the neutron lifetime anomaly. Then the DM-neutron elastic scattering cross section is obtained from t-channel ϕ exchange, $\chi n \to \phi \to \chi n$:

$$\sigma^{\rm elastic}_{\chi n\to\phi\to\chi n} = \sigma^{\rm elastic}_{\bar\chi n\to\phi\to\bar\chi n} \simeq \mathcal{O}(10^{-60})\ \text{cm}^2\,.$$

For $\sigma^{\rm ann}_{\bar\chi n}$, the dominant annihilation mode is ϕ + multipion, which depends on $m_\chi, m_{\tilde\chi}, m_\phi$. The detailed calculations in ref. [18] give

$$\sigma^{\rm ann}_{\bar\chi n}(v/c) \simeq \mathcal{O}(10^{-50} - 10^{-54})\ \text{cm}^2\,.$$

Both $\sigma^{\rm elastic}_{\chi n}$ and $\sigma^{\rm ann}_{\bar\chi n}$ contribute negligibly to NS heating since $\sigma^{\rm elastic}_{\bar\chi n} \ll \sigma_{\rm crit}$ and $\sigma^{\rm ann}_{\bar\chi n}(v/c) \ll \sigma^{\rm ann}_{\bar\chi\chi}(v/c)$. Therefore, in the following calculations, we conservatively fix $\sigma^{\rm elastic}_{\bar\chi n} = 0$ and $\sigma^{\rm ann}_{\bar\chi n}(v/c) = 10^{-54}$ cm^2 to estimate NS heating.

4.4 Results

The salient feature of this model is that neutrons can convert into χ inside the NS, which makes the NS composed of n and χ in most of the interesting parameter space. Then the DM self-scattering cross sections from the box diagrams in figure 6, that are significantly larger than the critical cross section $\sigma_{\rm crit}$, enhance the capture rate above the geometric limit. Consequently, the NS can be heated up to 1500 K. If further $\bar\chi - n$ and $\bar\chi - \chi$ annihilations are allowed, the NS temperature might reach 3100 K depending on the final state particles from annihilation.

We are interested in the parameter regions which can explain the neutron lifetime anomaly. The masses m_χ, m_ϕ, and $m_{\tilde\chi}$ in this model need to satisfy the relations [8]

$$\begin{aligned} &937.992\ \text{MeV} < m_\chi + m_\phi < 939.565\ \text{MeV}\,,\\ &937.992\ \text{MeV} < m_{\tilde\chi}\,,\\ &|m_\chi - m_\phi| < m_p + m_e = 938.783081\ \text{MeV}\,. \end{aligned} \tag{4.13}$$

JHEP07(2020)181

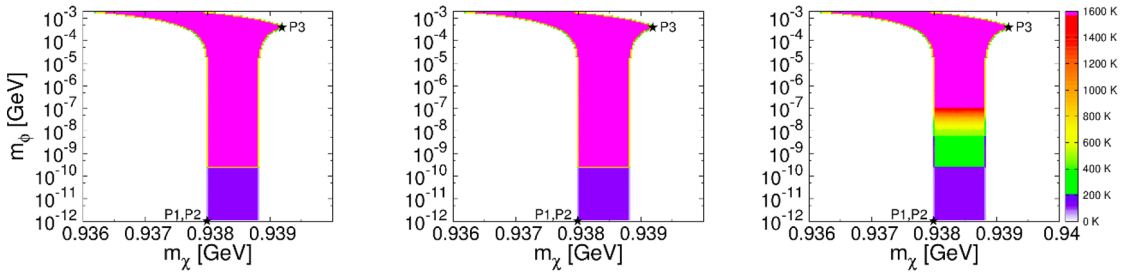

Figure 8. The minimum value of $T_{\rm obs}$ projected on the (m_χ, m_ϕ) plane when χ is DM. The temperature scale is shown on the right panel. The stars mark the three benchmark points **P1**, **P2**, and **P3**. Left-panel: attractive DM self-energy $-\frac{n_\chi^2}{2z'^2}$. Middle-panel: no DM self-energy. Right-panel: repulsive DM self-energy $+\frac{n_\chi^2}{2z'^2}$.

We choose three benchmark points of ref. [18],

$$\begin{aligned}
\mathbf{P1}: &\quad (m_\chi, m_\phi, m_{\tilde{\chi}}) = (937.992, 0, 937.992) \\
\mathbf{P2}: &\quad (m_\chi, m_\phi, m_{\tilde{\chi}}) = (937.992, 0, 2m_n) \\
\mathbf{P3}: &\quad (m_\chi, m_\phi, m_{\tilde{\chi}}) = (939.174, 0.391, 940.000)\,,
\end{aligned}$$

within the region. We fix $\lambda_\phi = 0.04$ to give the correct DM relic density [8], and $g_\chi = 4 \times 10^{-4}$ to alleviate the core-cusp problem [9].

Note that the light mediator ϕ is not stable and decays to diphotons by mixing with the SM Higgs via the $\mu H^\dagger H \phi$ term in eq. (4.1). Also, because of its tiny mixing with the SM Higgs, ϕ decouples from the primordial plasma before neutrino decoupling. Thus, ϕ does not contribute to the effective number of relativistic degrees of freedom in the early universe.

For the neutron dark decay model, the DM can be either $\bar{\chi}$ or χ, so we separately discuss these cases below.

4.4.1 χ is DM

In this subsection, we consider the case in which χ is DM, so there are no DM-neutron and DM-antiDM annihilation processes involved. Figure 8 shows the temperature increase in neutron stars older than 10^9 years in the parameter region of eq. (4.13). The panels from left to right correspond to attractive DM self-interaction, no DM self-interaction, and repulsive DM self-interaction scenarios. For each panel, the higher temperature region corresponds to a mixed phase of NS, and the lower temperature region corresponds to the neutron phase. A dramatic temperature change occurs at the boundary of these two phases. For attractive DM self-interactions and no DM self-interactions, the boundary occurs for $m_\phi \simeq 0.2\,\text{eV}$, which corresponds to $z \simeq 100\,\text{MeV}$. For repulsive DM self-interactions, the phase transition gradually occurs for 10 eV $\lesssim m_\phi \lesssim$ 100 eV, which corresponds to 5 GeV $\lesssim z \lesssim$ 50 GeV.

In the neutron phase, DM capture relies primarily on DM-neutron scattering. We can see that the NS temperature is always below 200 K. Because the DM-neutron cross section

JHEP07(2020)181

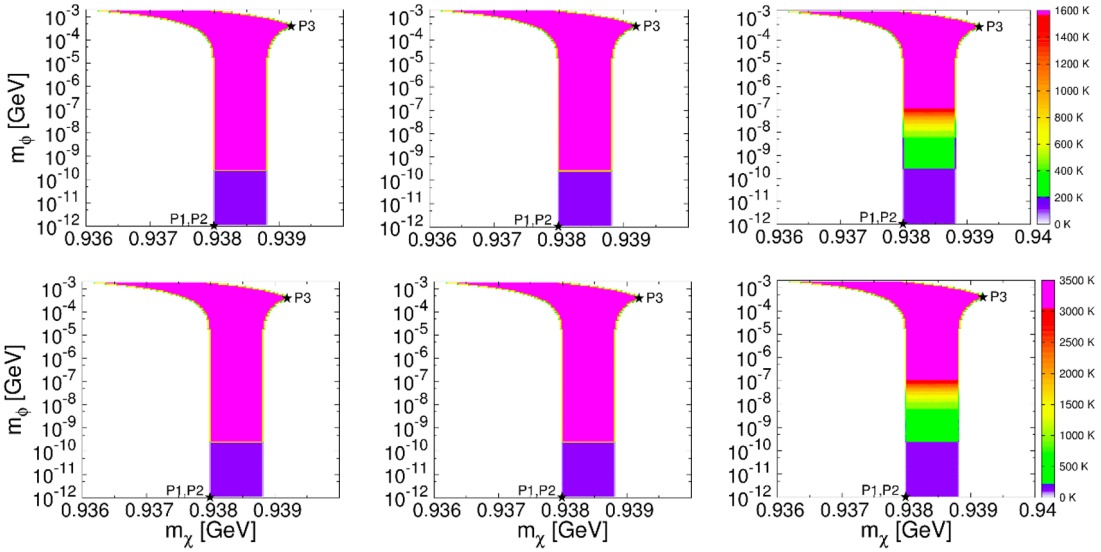

Figure 9. Same as figure 8 but $\bar{\chi}$ is DM. Upper-row: ϕ decay final states cannot be absorbed by the NS. Lower-row: ϕ decay final states are absorbed by the NS.

is too small to saturate the geometric limit, the kinematic recoil energy of halo DM cannot heat up the NS. In the mixed phase, there are substantial χ from neutron conversion inside the NS, and so, the DM self-capture kicks in and dramatically enhances the halo DM capture rate to the geometric limit. This results in an observed NS temperature of 1580 K, when the equilibrium condition $L_\gamma|_{T_{\rm sur}=1660\,{\rm K}} = C_c|_{\rm geom}(\langle E_R\rangle)$ is satisfied.

4.4.2 $\bar{\chi}$ is DM

In this subsection, we assume $\bar{\chi}$ is the DM candidate. Therefore, additional DM-neutron and DM-antiDM annihilation processes enhance the NS heating.

The DM-antiDM annihilation is through the $\chi\bar{\chi} \to \phi\phi$ process. Whether or not $\chi\bar{\chi} \to \phi\phi$ enhances the NS temperature, depends on whether or not the decay products of ϕ can be absorbed by the NS. If ϕ mixes with SM Higgs according to ref. [9], $\phi \to \gamma\gamma$ is the dominant channel, so that NS heating can be further enhanced. For scenarios in which ϕ decays into neutrinos or dark sector particles, DM-antiDM annihilation does not contribute to the heating process. In the upper and lower rows of figure 9, we separately show the two scenarios in which the final state particles are absorbed or not absorbed by the NS.

In figure 9, for each panel, there are higher and lower temperature regions respectively corresponding to the mixed and neutron phases. The upper row of figure 9, which shows the neutron phase, has an additional DM-neutron annihilation process (compared to the χ DM case) to heat up the NS. However, its contribution is insignificant and the observed temperature is below 200 K. In the mixed phase, again, the substantial component of χ in the NS and large DM-antiDM scattering help the capture rate to reach the geometric limit, but the additional DM-χ annihilation cannot heat up the NS, because the annihilation final states cannot been absorbed. The result is that kinetic heating raises the NS temperature to 1580 K.

JHEP07(2020)181

In the mixed phase, the DM-antiDM annihilation process enhances the NS observed temperature up to 3100 K corresponding to a surface temperature of 3440 K; see the lower panel of figure 9. This occurs when the equilibrium condition $L_\gamma|_{T_{\rm sur}=3440\,\rm K} = C_c|_{\rm geom}(\langle E_R\rangle + 2m_\chi)$ is satisfied. But in the neutron phase, the temperature is lower than 200 K because there is no χ component from neutron conversion to annihilate with DM $\bar{\chi}$.

5 Quark vector current portal dark matter

We consider Dirac DM with mass around a GeV that couples to quarks through a vector current interaction. It is difficult for current DM direct detection experiments to probe this scenario because the recoil energy is much lower than the typical detector threshold. However, the leading DM annihilation final state is $\pi^+\pi^-$, which produces MeV photons that can be observed by near future instruments that will fill in the "MeV-gap" in the cosmic photon spectrum [10, 11]. Through the quark vector current, we also expect substantial DM-neutron scattering that will enable a NS to capture halo DM, which in turn will heat the NS.

5.1 DM-nucleon scattering cross section

Consider a Dirac fermion DM particle χ that couples to quarks through a vector-vector current,

$$\mathcal{L}_{\rm int} = \sum_{q=u,d,s} \frac{\alpha_q}{\Lambda^2}\bar{\chi}\gamma^\mu\chi\bar{q}\gamma_\mu q\,, \tag{5.1}$$

where α_q are the coupling strengths and Λ is a cutoff scale. To describe DM capture by a NS, the DM-neutron scattering cross section should be calculated in the relativistic limit, since the DM particles are accelerated close to the speed of light. The DM-neutron and DM-proton cross sections are given by [27, 39]

$$\frac{d\sigma_{\chi n,p}(s,t)}{d\cos\theta_{\rm cm}} = \frac{c_{\chi n,p}}{\Lambda^4}\frac{2(\bar{\mu}^2+1)^2m_\chi^4 - 4(\bar{\mu}^2+1)\bar{\mu}^2 s m_\chi^2 + \bar{\mu}^4(2s^2+2st+t^2)}{16\pi\bar{\mu}^4 s}|F_n(E_R)|^2\,, \tag{5.2}$$

where $\theta_{\rm cm}$ is the scattering angle in the center mass frame and $\bar{\mu} \equiv m_\chi/m_n \simeq m_\chi/m_p$. Here, $c_{\chi p,n} = (\alpha_u B_u^{p,n} + \alpha_d B_d^{p,n})^2$, with the integrated nuclear form-factors, $B_u^p = B_d^n = 2$ and $B_u^n = B_d^p = 1$. The nucleon form factor is $|F_n(E_R)|^2 = \exp[-E_R/(0.114\ \text{GeV})]$ [39], where E_R is the recoil energy in the initial n or p rest frame. For DM capture by a NS, in the initial nucleon rest frame, the energy of DM due to gravitational acceleration is $m_\chi/\sqrt{1-\omega^2} \simeq m_\chi/\sqrt{\bar{B}}$, where we have neglected the thermal motion of the DM. The expressions for the other kinematic variables are

$$\begin{aligned} s &= m_\chi^2 + m_n^2 + 2m_\chi m_n/\sqrt{\bar{B}}\,,\\ t &= -2|\overrightarrow{p_0}|^2(1-\cos\theta_{\rm cm})\,,\\ E_R &= \frac{|\overrightarrow{p_0}|^2}{m_{n,p}}(1-\cos\theta_{\rm cm})\,,\\ |\overrightarrow{p_0}|^2 &= \frac{(1-\bar{B})m_\chi m_n\bar{\mu}}{\bar{B}+2\sqrt{\bar{B}}\bar{\mu}+\bar{B}\bar{\mu}^2} \end{aligned} \tag{5.3}$$

where $|\overrightarrow{p_0}| = \frac{\sqrt{s}}{2}\lambda^{1/2}(1, m_\chi^2/s, m_n^2/s)$ and $\lambda(x,y,z) \equiv x^2+y^2+z^2-2xy-2xz-2yz$.

JHEP07(2020)181

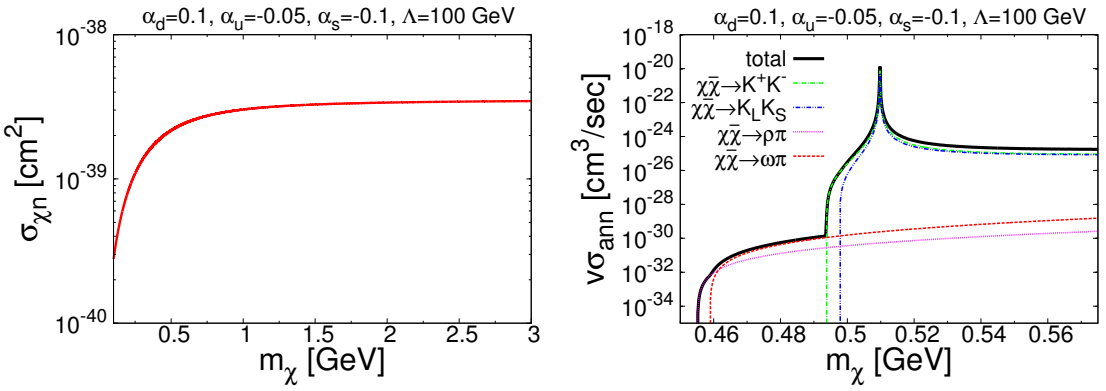

Figure 10. Left-panel: The DM-neutron scattering cross section in the relativistic limit for DM capture by a NS with $M = 1.44 M_\odot$ and $R = 10.6$ km. Right-panel: The $\chi\bar{\chi}$ annihilation cross sections for $\sqrt{s} \leq 1.15\,\text{GeV}$ including interference effects.

An example of the DM-neutron scattering cross section for DM capture by a NS is provided in figure 10. By choosing couplings strengths $\alpha_q = \mathcal{O}(10^{-4})$ and $\Lambda = 100\,\text{GeV}$, the DM-neutron cross section is larger than the critical cross section. Therefore, we expect the corresponding DM capture rate to reach the geometric limit and an old NS temperature can be heated up to 1500 K. The sensitivity provided by NS heating is significantly greater than that from future observations of MeV cosmic photons by e-ASTROGAM, AMEGO and APT, which are sensitive to $\alpha_q/\Lambda \sim \mathcal{O}(1)/100\,\text{GeV}$ [10].

5.2 Chiral Lagrangian and DM annihilation

We now calculate NS heating due to DM-antiDM annihilation. At the GeV scale, DM-quark vector current interactions can be described by Chiral perturbation theory, such that the DM annihilate into pseudoscalar or vector mesons. We focus on $\sqrt{s} \lesssim 1.15\,\text{GeV}$, so that we only need to include the $\chi\bar{\chi} \to K^+K^-, K_L K_S, \rho\pi, \omega\pi$ channels.

The Feynman rules for GeV DM couplings to low-energy QCD pseudoscalar meson and vector meson can be found in appendix B of ref. [10]. Then the vector meson propagator $< 0|T(\rho_{\mu\nu}, \rho_{\alpha\beta})|0 >$ is [40]

$$\frac{g_{\mu\alpha}g_{\nu\beta}(m_\rho^2 - k^2) + g_{\mu\alpha}k_\nu k_\beta - g_{\mu\beta}k_\nu k_\alpha - g_{\nu\alpha}g_{\mu\beta}(m_\rho^2 - k^2) - g_{\nu\alpha}k_\mu k_\beta + g_{\nu\beta}k_\mu k_\alpha}{(m_\rho^2)(m_\rho^2 - k^2 - i\varepsilon)}\,, \quad (5.4)$$

and the polarization of $\rho_{\mu\nu}$ is $[k_\mu\epsilon_\nu(k) - k_\nu\epsilon_\mu(k)]/m_\rho$. The polarization sum between $\rho_{\mu\nu}$ and $\rho_{\mu'\nu'}$ is given by $\left[k_\mu k_{\nu'}g_{\nu\mu'} + k_\nu k_{\mu'}g_{\mu\nu'} - \left(k_\mu k_{\mu'}g_{\nu\nu'} + k_\nu k_{\nu'}g_{\mu\mu'}\right)\right]/m_\rho^2$. Using the ρ propagator in eq. (5.4) and the $\chi\bar{\chi}\rho$, $K^+K^-\rho$ vertices from appendix B of ref. [10], the amplitude squared for $\chi(p)\bar{\chi}(p') \to \rho \to K^+(k)K^-(k')$ is

$$\frac{1}{4}\sum|M|^2 = (\alpha_d - \alpha_u)^2\left\{\frac{4f_V^2 h_p}{2\Lambda^2 F^2}\right\}^2 \frac{1}{(s - m_\rho^2)^2 + m_\rho^2\Gamma_\rho^2}$$
$$\times\, 2\left[s^2 - 4s\,m_K^2 - (u-t)^2\right]\left[(u+t) - 2(m_\chi^2 + m_K^2)\right]^2\,, \quad (5.5)$$

JHEP07(2020)181

where $s \equiv (p+p')^2 = (k+k')^2$, $t \equiv (p-k')^2 = (k-p')^2$, $u \equiv (p-k)^2 = (k'-p')^2$, and the values for f_V, h_p, and F can be found in ref. [10] In terms of the Mandelstam variables,

$$u - t = -4|\overrightarrow{p}||\overrightarrow{k}|\cos\theta\,,$$
$$u + t = -2(|\overrightarrow{p}|^2 + |\overrightarrow{k}|^2)\,,$$

where θ is the angle between $\overrightarrow{p}$ and $\overrightarrow{k}$, and $|\overrightarrow{p}| = \frac{\sqrt{s}}{2}\sqrt{1-\frac{4m_\chi^2}{s}}$, $|\overrightarrow{k}| = \frac{\sqrt{s}}{2}\sqrt{1-\frac{4m_K^2}{s}}$. In the threshold limit, $s \to 4m_\chi^2 \Rightarrow u - t = 0$ and $u + t = -2(m_\chi^2 - m_K^2)$. Then the amplitude squared can be simplified to

$$\frac{1}{4}\sum|M|^2 = (\alpha_d - \alpha_u)^2\left\{\frac{4f_V^2 h_p}{2\Lambda^2 F^2}\right\}^2 \frac{1}{(4m_\chi^2 - m_\rho^2)^2 + m_\rho^2\Gamma_\rho^2} \times 512\, m_\chi^8\left(1 - \frac{m_K^2}{m_\chi^2}\right)\,. \tag{5.6}$$

The total and partial $\bar{\chi}\chi$ annihilation cross sections are shown in figure 10 including interference effects. For $\sqrt{s} > 1.15\,\mathrm{GeV}$, other channels are kinematically viable, like a glueball with neutral pions. Because the calculation of glueball emission is beyond the scope of this work, we only consider the DM annihilation cross section for $\sqrt{s} \lesssim 1.15\,\mathrm{GeV}$. Moreover, as long as the DM annihilation rate is large enough to maintain equilibrium between the DM capture rate and depletion rates, including the new channels do not further increase the temperature of the NS. Without including the DM annihilation channels above $\sqrt{s}$ =1.15 GeV, we still obtain a conservative estimate of NS heating for DM masses above 0.575 GeV.

5.3 Results

In figure 11, we shown the observed temperature of the NS due to the vector-vector current couplings to quarks in eq. (5.1). For α_u or α_d larger than $O(10^{-4})$, DM capture heats up the NS to more than 1480 K, which is shown by the black curve. However, for $\alpha_u = -2\alpha_d$ the DM-neutron scattering cross section vanishes, and the NS does not get heated. This feature is indicated by the dashed line in figure 11.

In figure 12, we vary α_s and $\alpha_u + \alpha_d$, and fix $\alpha_u = \alpha_d$, $\Lambda = 100\,\mathrm{GeV}$ and $m_\chi = 1\,\mathrm{GeV}$. Clearly, $T_{\rm obs}$ is insensitive to the parameter α_s, which modifies $v\sigma^{\rm ann}$, but not $\sigma_{\chi n}^{\rm elastic}$; α_s only affects $\mathcal{O}(100)$ K temperatures. We may understand the features of figure 12 as follows. First, focus on the region of $T_{\rm obs}$ above 1000 K, where $\sigma_{\chi n}^{\rm elastic}$ is close to $\sigma_{\rm crit} \simeq 2\times10^{-45}\,\mathrm{cm}^2$ and the DM capture rate C_c reaches the geometric limit. This corresponds to $\alpha_u \simeq \alpha_d \simeq 4\times10^{-5}$ which gives a DM annihilation cross section, $v\sigma^{\rm ann} \simeq \mathcal{O}(10^{-33})\,\mathrm{cm}^3/\mathrm{s}$, which is six orders of magnitude larger than $v\sigma^{\rm ann}|_{\rm sat} \simeq \mathcal{O}(10^{-39})\,\mathrm{cm}^3/\mathrm{s}$. α_s only alters $v\sigma^{\rm ann}$ within a similar magnitude, but cannot suppress it down to $v\sigma^{\rm ann}|_{\rm sat}$. Thus, for $T_{\rm obs}$ around 1000 K, $T_{\rm obs}$ is insensitive to α_s.

However, the situation is different when the final $T_{\rm obs}$ is of $\mathcal{O}(100)$ K, which corresponds to much smaller values of C_c and $\sigma_{\chi n}^{\rm elastic}$. Take $C_c = 10^{-4}\times C_c|_{\rm geom}$ as an example. This corresponds to $\sigma_{\chi n}^{\rm elastic} = 2\times10^{-49}\,\mathrm{cm}^2$ and $\alpha_u \simeq \alpha_d \simeq 4\times10^{-7}$, which gives

JHEP07(2020)181

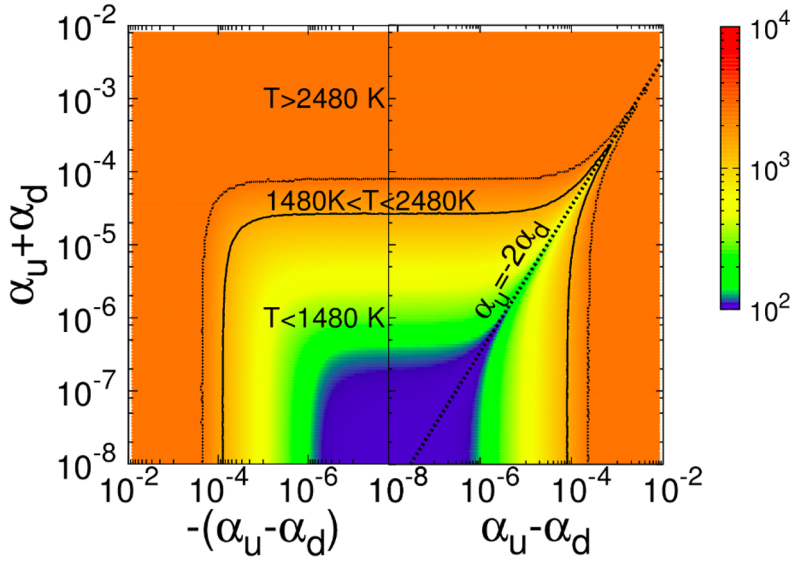

Figure 11. $T_{\rm obs}$ (in K) in the vector portal DM framework by varying α_u and α_d. We fix $\alpha_s = 0$, $\Lambda = 100\,\text{GeV}$ and $m_\chi = 1\,\text{GeV}$.

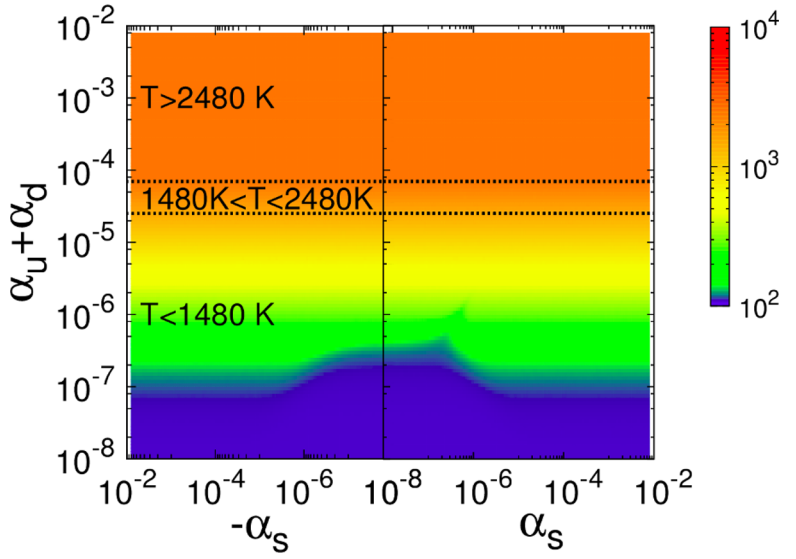

Figure 12. $T_{\rm obs}$ (in K) in the vector portal DM framework by varying α_s and $\alpha_u + \alpha_d$, while fixing $\alpha_u = \alpha_d$, $\Lambda = 100\,\text{GeV}$ and $m_\chi = 1\,\text{GeV}$.

$v\sigma^{\rm ann} \simeq \mathcal{O}(10^{-37})$, which is much smaller than the saturating annihilation cross section, $v\sigma^{\rm ann}|_{\rm sat} \simeq \mathcal{O}(10^{-35})$. This means that increasing $v\sigma^{\rm ann}$ by varying α_s enhances the final NS temperature $T_{\rm obs}$. This behavior at $\mathcal{O}(100)$ K is evident from the dark blue region in figure 12. For $\alpha_u + \alpha_d = 2 \times 10^{-7}$, increasing $|\alpha_s|$ from 10^{-8} to 10^{-5} raises $T_{\rm obs}$, which plateaus for $|\alpha_s| > 10^{-5}$. The little spike at $\alpha_s \simeq 3 \times 10^{-7}$ is due to destructive interference between the DM annihilation channels.

JHEP07(2020)181

6 Summary

We have investigated NS heating by the capture of GeV-mass DM. We discussed the generic scenario that the NS could be in a mixed phase composed of both neutrons and a substantial population of DM from neutron conversion. In this case, the geometric limit of the DM capture rate can be saturated through DM self-interactions without DM-neutron interactions.

A NS can be in a mixed phase in the neutron dark decay model (that explains the neutron lifetime anomaly), because neutrons are able to convert to DM. We demonstrated that a NS in mixed phase can be stable and its mass can be as heavy as $2M_\odot$ by solving the equation of state and Tolman-Oppenheimer-Volkoff equations.

To illustrate the effect of DM capture on NS heating, we chose the above mentioned neutron dark decay model and the quark vector current portal framework. For the neutron dark decay model, since the DM self-scattering cross section is crucial to estimate the DM capture rate, we calculated the tree-level and one-loop box diagram contributions. In the mixed phase of a NS, DM self-scattering can enhance the DM capture rate up to the geometric limit without DM-neutron interactions. We find that for $m_\phi \gtrsim 100\,\text{eV}$, the sensitivity of near future infrared instruments is greater than afforded by multi-pion signatures at Super-Kamiokande, Hyper-Kamionkande, and DUNE.

For quark vector portal DM, since the NS is in the neutron phase, halo DM is captured only via DM-neutron interactions. We find that the capture rate is close to the geometric limit for $\alpha_{u,d} \gtrsim \mathcal{O}(10^{-4})$, in which case the NS is heated to $\sim$ 1500 K. This is four orders of magnitude more sensitive than the detection of MeV cosmic gamma rays by e-ASTROGAM, AMEGO and APT, which are sensitive to $\alpha_{u,d} \simeq \mathcal{O}(1)$ [10]. We also find that NS heating is not sensitive to α_s, unless future telescopes can observe NS temperatures of around 100 K.

A NS that is heated to 1480 K produces a photon spectrum that is peaked at about 1–2 μm and has a spectral flux density of $\simeq 0.5$ nJy if the NS is at a distance of 10 pc from Earth. This is near the optimal sensitivity of the upcoming infrared telescopes, JWST, Thirty Meter Telescope, and European Extremely Large Telescope [3]. JWST is closest to completion, and is expected to reach $\mathcal{O}(10)$ signal-to-noise for $\mathcal{O}(10)$ nJy in a typical integration time of 10^4 seconds [41]. A 2480 K NS at 10 pc (50 pc) can be detected by JWST in 2000 seconds ($\mathcal{O}(10^6)$ seconds).

Acknowledgments

We thank J. Kumar and X. Tata for discussions. W.-Y.K. and P.-Y.T. thank the National Center of Theoretical Sciences, Taiwan, for its hospitality. D.M. thanks the Aspen Center for Physics (which is supported by U.S. NSF Grant No. PHY-1607611) for its hospitality while this work was in progress. D.M. is supported in part by the U.S. DOE under Grant No. de-sc0010504.

JHEP07(2020)181

References

[1] S.D. McDermott, H.-B. Yu and K.M. Zurek, *Constraints on Scalar Asymmetric Dark Matter from Black Hole Formation in Neutron Stars*, *Phys. Rev. D* **85** (2012) 023519 [arXiv:1103.5472] [INSPIRE].

[2] T. Güver, A.E. Erkoca, M. Hall Reno and I. Sarcevic, *On the capture of dark matter by neutron stars*, *JCAP* **05** (2014) 013 [arXiv:1201.2400] [INSPIRE].

[3] M. Baryakhtar, J. Bramante, S.W. Li, T. Linden and N. Raj, *Dark Kinetic Heating of Neutron Stars and An Infrared Window On WIMPs, SIMPs and Pure Higgsinos*, *Phys. Rev. Lett.* **119** (2017) 131801 [arXiv:1704.01577] [INSPIRE].

[4] C.-S. Chen and Y.-H. Lin, *Reheating neutron stars with the annihilation of self-interacting dark matter*, *JHEP* **08** (2018) 069 [arXiv:1804.03409] [INSPIRE].

[5] R. Garani, Y. Genolini and T. Hambye, *New Analysis of Neutron Star Constraints on Asymmetric Dark Matter*, *JCAP* **05** (2019) 035 [arXiv:1812.08773] [INSPIRE].

[6] N.F. Bell, G. Busoni and S. Robles, *Capture of Leptophilic Dark Matter in Neutron Stars*, *JCAP* **06** (2019) 054 [arXiv:1904.09803] [INSPIRE].

[7] R. Garani and J. Heeck, *Dark matter interactions with muons in neutron stars*, *Phys. Rev. D* **100** (2019) 035039 [arXiv:1906.10145] [INSPIRE].

[8] B. Fornal and B. Grinstein, *Dark Matter Interpretation of the Neutron Decay Anomaly*, *Phys. Rev. Lett.* **120** (2018) 191801 [*Erratum ibid.* **124** (2020) 219901] [arXiv:1801.01124] [INSPIRE].

[9] B. Grinstein, C. Kouvaris and N.G. Nielsen, *Neutron Star Stability in Light of the Neutron Decay Anomaly*, *Phys. Rev. Lett.* **123** (2019) 091601 [arXiv:1811.06546] [INSPIRE].

[10] D. Berger, A. Rajaraman and J. Kumar, *Dark Matter Through the Quark Vector Current Portal*, arXiv:1903.10632 [INSPIRE].

[11] J. Kumar, *Indirect Detection of Sub-GeV Dark Matter Coupling to Quarks*, *Phys. Rev. D* **98** (2018) 116009 [arXiv:1808.02579] [INSPIRE].

[12] Particle Data Group collaboration, *Review of Particle Physics*, *Chin. Phys. C* **40** (2016) 100001 [INSPIRE].

[13] J. Byrne and P.G. Dawber, *A Revised Value for the Neutron Lifetime Measured Using a Penning Trap*, *Europhys. Lett.* **33** (1996) 187 [INSPIRE].

[14] A.T. Yue et al., *Improved Determination of the Neutron Lifetime*, *Phys. Rev. Lett.* **111** (2013) 222501 [arXiv:1309.2623] [INSPIRE].

[15] A. Pichlmaier, V. Varlamov, K. Schreckenbach and P. Geltenbort, *Neutron lifetime measurement with the UCN trap-in-trap MAMBO II*, *Phys. Lett. B* **693** (2010) 221 [INSPIRE].

[16] A. Steyerl, J.M. Pendlebury, C. Kaufman, S.S. Malik and A.M. Desai, *Quasielastic scattering in the interaction of ultracold neutrons with a liquid wall and application in a reanalysis of the Mambo I neutron-lifetime experiment*, *Phys. Rev. C* **85** (2012) 065503 [INSPIRE].

JHEP07(2020)181

[17] S. Arzumanov et al., *A measurement of the neutron lifetime using the method of storage of ultracold neutrons and detection of inelastically up-scattered neutrons*, *Phys. Lett. B* **745** (2015) 79 [INSPIRE].

[18] W.-Y. Keung, D. Marfatia and P.-Y. Tseng, *Annihilation signatures of neutron dark decay models in neutron oscillation and proton decay searches*, *JHEP* **09** (2019) 053 [arXiv:1905.03401] [INSPIRE].

[19] S. Tulin, H.-B. Yu and K.M. Zurek, *Resonant Dark Forces and Small Scale Structure*, *Phys. Rev. Lett.* **110** (2013) 111301 [arXiv:1210.0900] [INSPIRE].

[20] CRESST collaboration, *First results from the CRESST-III low-mass dark matter program*, *Phys. Rev. D* **100** (2019) 102002 [arXiv:1904.00498] [INSPIRE].

[21] A.R. Zentner, *High-Energy Neutrinos From Dark Matter Particle Self-Capture Within the Sun*, *Phys. Rev. D* **80** (2009) 063501 [arXiv:0907.3448] [INSPIRE].

[22] C. Kouvaris, *WIMP Annihilation and Cooling of Neutron Stars*, *Phys. Rev. D* **77** (2008) 023006 [arXiv:0708.2362] [INSPIRE].

[23] S.L. Shapiro and S.A. Teukolsky, *Black holes, white dwarfs, and neutron stars: The physics of compact objects*, Wiley, New York, U.S.A. (1983).

[24] D. Page, J.M. Lattimer, M. Prakash and A.W. Steiner, *Minimal cooling of neutron stars: A new paradigm*, *Astrophys. J. Suppl.* **155** (2004) 623 [astro-ph/0403657] [INSPIRE].

[25] E.H. Gudmundsson, C.J. Pethick and R.I. Epstein, *Neutron star envelopes*, *Astrophys. J.* **259** (1982) L19.

[26] E.H. Gudmundsson, C.J. Pethick and R.I. Epstein, *Structure of neutron star envelopes*, *Astrophys. J.* **272** (1983) 286.

[27] N.F. Bell, G. Busoni and S. Robles, *Heating up Neutron Stars with Inelastic Dark Matter*, *JCAP* **09** (2018) 018 [arXiv:1807.02840] [INSPIRE].

[28] S. Nussinov, *Technocosmology: Could A Technibaryon Excess Provide A 'natural' Missing Mass Candidate?*, *Phys. Lett. B* **165** (1985) 55 [INSPIRE].

[29] D.E. Kaplan, M.A. Luty and K.M. Zurek, *Asymmetric Dark Matter*, *Phys. Rev. D* **79** (2009) 115016 [arXiv:0901.4117] [INSPIRE].

[30] M. Ibe, S. Matsumoto and T.T. Yanagida, *The GeV-scale dark matter with B-L asymmetry*, *Phys. Lett. B* **708** (2012) 112 [arXiv:1110.5452] [INSPIRE].

[31] D. McKeen, A.E. Nelson, S. Reddy and D. Zhou, *Neutron stars exclude light dark baryons*, *Phys. Rev. Lett.* **121** (2018) 061802 [arXiv:1802.08244] [INSPIRE].

[32] J. Heeck, *Unbroken B-L symmetry*, *Phys. Lett. B* **739** (2014) 256 [arXiv:1408.6845] [INSPIRE].

[33] S. Gandolfi, J. Carlson and S. Reddy, *The maximum mass and radius of neutron stars and the nuclear symmetry energy*, *Phys. Rev. C* **85** (2012) 032801 [arXiv:1101.1921] [INSPIRE].

[34] J.M. Cline and J.M. Cornell, *Dark decay of the neutron*, *JHEP* **07** (2018) 081 [arXiv:1803.04961] [INSPIRE].

[35] F. Douchin and P. Haensel, *A unified equation of state of dense matter and neutron star structure*, *Astron. Astrophys.* **380** (2001) 151 [astro-ph/0111092] [INSPIRE].

JHEP07(2020)181

[36] T. Hahn and M. Pérez-Victoria, *Automatized one loop calculations in four-dimensions and D-dimensions*, *Comput. Phys. Commun.* **118** (1999) 153 [hep-ph/9807565] [INSPIRE].

[37] P.B. Pal, *Representation-independent manipulations with Dirac spinors*, physics/0703214 [INSPIRE].

[38] S.A. Raby and G. West, *A Simple Solution to the Solar Neutrino and Missing Mass Problems*, *Nucl. Phys. B* **292** (1987) 793 [INSPIRE].

[39] J.L. Feng, J. Smolinsky and P. Tanedo, *Detecting dark matter through dark photons from the Sun: Charged particle signatures*, *Phys. Rev. D* **93** (2016) 115036 [*Erratum ibid.* **96** (2017) 099903] [arXiv:1602.01465] [INSPIRE].

[40] G. Ecker, J. Gasser, A. Pich and E. de Rafael, *The Role of Resonances in Chiral Perturbation Theory*, *Nucl. Phys. B* **321** (1989) 311 [INSPIRE].

[41] *JWST Pocket Guide*, https://www.stsci.edu/files/live/sites/www/files/home/jwst/instrumentation/_documents/jwst-pocket-guide.pdf.

JHEP07(2020)181